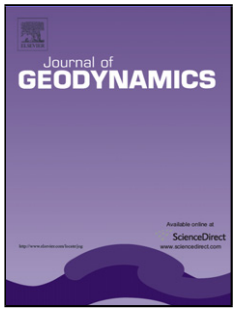

Tectonically controlled carbonate-seated maar-diatreme volcanoes: the case of the Volsci Volcanic Field, central Italy

G.L. Cardello (Conceptualization) (Investigation) (Data curation) (Formal analysis) (Methodology) (Writing - original draft), L. Consorti (Investigation) (Data curation) (Formal analysis), D.M. Palladino (Data curation) (Writing - review and editing) (Visualization), E. Carminati (Funding acquisition) (Resources) (Supervision) (Writing - review and editing) (Project administration), M. Carlini (Software) (Data curation) (Validation), C. Doglioni (Funding acquisition) (Writing - review and editing) (Supervision)

PII: S0264-3707(20)30105-8

DOI: https://doi.org/10.1016/j.jog.2020.101763

Reference: GEOD 101763

To appear in: *Journal of Geodynamics*

Received Date: 24 February 2020

Revised Date: 10 June 2020

Accepted Date: 14 June 2020

Please cite this article as: Cardello GL, Consorti L, Palladino DM, Carminati E, Carlini M, Doglioni C, Tectonically controlled carbonate-seated maar-diatreme volcanoes: the case of the Volsci Volcanic Field, central Italy, *Journal of Geodynamics* (2020), doi: https://doi.org/10.1016/j.jog.2020.101763

Tectonically controlled carbonate-seated maar-diatreme volcanoes: the case of the Volsci Volcanic Field, central Italy

G. L. Cardello[1], L. Consorti[2], D. M. Palladino[1], E. Carminati[1], M. Carlini[3], C. Doglioni[1]

[1] Department of Earth Sciences, Sapienza University of Rome, Italy.

[2] Department of Mathematics and Geosciences, University of Trieste, Italy.

[3] Department of Earth Sciences, University of Bologna, Italy.

Corresponding author: G. Luca Cardello (luca.cardello@uniroma1.it)

graphical abstract

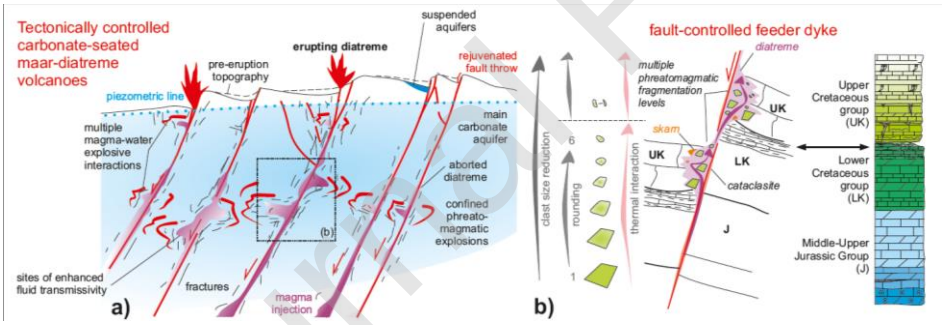

Abstract

Quaternary carbonate-seated maar-diatremes in the Volsci Range are one of the most intriguing products of the west-directed subduction of the Adriatic slab that drove the development of the Apennine mountain belt in Central Italy. The Volsci Volcanic Field is characterized by phreatomagmatic surge deposits, rich in accidental carbonate lithics, and subordinate

Strombolian scoria fall deposits and lava flows, locally sourced from some tens of monogenetic eruptive centers (at least fifty tuff rings and scoria cones). We investigate the subsurface maar-diatreme processes in terms of relationships between faulting and explosive magma-water interaction, as well as the distribution pattern of the eruptive centers. With this aim, we present the following new data: i) description of the fold-and-thrust belt structure and associated eruptive centers, ii) componentry of volcanic rock-types, iii) determination of grain-size, degrees of whiteness and roundness of carbonate lithic inclusions, iv) micropaleontological analysis of carbonate lithics. We show that the clustering of eruptive centers is controlled by tectonic features. A first order control is tentatively related to crustal laceration and deep magma injection along a ENE-trending Quaternary lateral tear in the slab and to Mesozoic rift-related normal faults. A second-order control is provided by orogenic structures (mainly thrust and extensional faults). In particular, magma-water explosive interaction occurred at multiple levels (< 2.3 km depth), depending on the structural and hydrogeologic setting of the Albian-Cenomanian carbonates, which are intersected by high-angle faults. The progressive comminution, rounding and whitening of entrained carbonate lithics allows us to trace multistage diatreme processes. Finally, our study bears implications on volcanic hazard assessment in the region.

1. Introduction

Fault-controlled volcanic fields may be composed of monogenetic magmatic and/or phreatomagmatic eruptive centers. The latter are defined as maar-diatreme volcanoes, forming as the result of the explosive interaction between rising magma and groundwater, interpreted in the frame of molten fuel-coolant interaction (e.g.; Sheridan & Wohletz, 1983; Lorenz, 1986; Sottili et al., 2009; Taddeucci et al., 2010; White & Ross, 2011; Valentine & White, 2012; Graettinger et al., 2014; Valentine et al., 2015 ; Németh & Kósik, 2020). After

scoria cones, monogenetic maar-diatreme volcanoes are the second most common volcano type (Lorenz, 1987; Wohletz & Heiken, 1992). They occur as craters cutting into the pre-eruption land surface, while the co-genetic eruptive deposits are organized in low-profile tephra rings. Maar crater sizes increase parallel to the amounts of juvenile vs. lithic products, within a spectrum of explosive volcanic depressions, ranging from phreatic to large caldera end-members (Palladino et al., 2015; Graettinger, 2018): i.e., the volume of involved magma is null for phreatic explosion craters (or hydrothermal craters) and becomes progressively more relevant towards large overpressure calderas dominated by the collapse of the magma chamber roof.

Recent conceptual models, supported by evidence from experiments, numerical modeling and field data, describe maar-diatremes and associated tephra rings as derived from sub-surface phreatomagmatic explosions occurring at multiple depths (Valentine et al., 2015), also possibly controlled by the downward migration of a groundwater drawdown cone (Lorenz, 1986; Lorenz et al., 2017). Churning and mixing of diatreme fill may occur through a combination of upward-directed debris jets and downward subsidence (e.g., McClintock & White, 2006; Ross & White, 2006; Lefebvre et al., 2013; Andrews et al., 2014; Graettinger et al., 2014; Sweeney & Valentine, 2015; Valentine et al., 2015). Field and textural analyses of the ejected material provide crucial information to unravel the depths and thermal conditions of magma-aquifer interaction (Sottili et al., 2009, 2012; Danese & Mattei, 2010), with inferences on the subsurface diatreme-wall rock fabric.

The Quaternary potassic volcanoes of the Roman Province (Peccerillo, 2005), aligned along a NW-SE direction on the Tyrrhenian Sea margin of Central Italy (Fig. 1), are known worldwide as sites of magma-carbonate wall rock interaction. They involve a full range of eruption styles and magnitudes, from lava flows to large-scale caldera-forming explosive events,

also including phreatomagmatic events resulting from the explosive interaction with carbonate aquifers (e.g., Freda et al., 1997, 2011; Sottili et al., 2010; Giordano et al., 2014).

Here we address Quaternary carbonate-seated maar-diatremes in the northern area of the Volsci Range (VR in the following, part of the Central Apennines; Fig. 1), aiming at defining the sites and depths of carbonate aquifer-magma interactions in the context of a fold-and-thrust belt affected by post-contractional normal faulting and magma ascent. Different from the nearby Colli Albani Volcanic District, where the interaction involved Mesozoic pelagic to base-of-slope carbonates (Funiciello & Parotto, 1978; Giordano et al., 2006; Sottili et al., 2009; Danese & Mattei, 2010; De Benedetti et al., 2010), the VR area provides evidence of repeated interaction between primitive potassic magmas (i.e., also including K-basalts) and Meso-Cenozoic shallow-water platform carbonates. An intriguing aspect is the episodic character and the small erupted volume (compared with the nearby volcanic districts of the Roman Province) of this volcanism and the primitive magma composition, suggesting the fast ascent of small magma batches from the mantle with very limited differentiation (e.g., Boari et al., 2009; Centamore et al., 2010). The eruptive centers in the northern VR are part of the Volsci Volcanic Field (see Section 2), which represents a good example of a "tectonically controlled volcanic field" (*sensu* Valentine and Perry, 2007), where the very low magma flux is a passive byproduct of regional tectonic strain. We investigate the relationships between phreatomagmatism and faulting, with general insights on the Adriatic subduction dynamics. Finally, considering the young age of volcanic activity (e.g., up to 230 ka; Centamore et al., 2010 and reference therein), the present work bears implications on hazard assessment in a region inhabited by 0.4 million people (https://www.regione.lazio.it/).

2. Geological Setting

Since at least the Tortonian time (ca. 11 Ma), the west-directed subduction of the Adriatic slab drove the development of the VR area of the Apennine mountain belt and the Tyrrhenian Sea back-arc basin (Doglioni,1991, Molli, 2008; Rosenbaum et al., 2008; Carminati et al. 2014; Beaudoin et al., 2017 and references therein). During the Quaternary, the Tyrrhenian Sea margin of central Italy was affected by the potassic magmatism of the Roman and Campanian provinces (Roman Co-magmatic Region; Washington, 1906), also including the presently active Campi Flegrei and Somma-Vesuvius volcanoes.

Overall, the Apennines are characterized by the differential retreat of the W-directed subducting Adriatic-Ionian plate relative to their northern and southern arcs (e.g., Doglioni, 1991; Carminati and Doglioni, 2012; Rosenbaum and Piana Agostinetti, 2015 and reference therein). The VR is one of the most internal chains of the NW-trending Apennine fold-and-thrust belt (Cosentino et al., 2002; Centamore et al., 2007), and is comprised between the NNE-striking Ancona-Anzio and Ortona-Roccamonfina major tectonic lines (Fig.1). These tectonic lineaments recorded polyphase tectonic activity, which initiated at least in early Jurassic time with the rifting stage that produced the boundary between carbonate basin and platform domains (Centamore et al., 2002). In particular, the Ancona–Anzio lineament (e.g., Castellarin et al., 1982; Butler et al., 2006 and references therein) was re-activated during late Miocene time as a transpressive front (i.e., Olevano–Antrodoco–Sibillini line; Pizzi & Galadini, 2009).

The VR comprises three major mountain groups (Lepini, Ausoni and Aurunci Mts.) located between the Colli Albani Volcanic District to the northwest and the Roccamonfina volcano to the southeast. The VR is punctuated by the occurrence of volcanic deposits of Pleistocene age from both nearby potassic volcanic districts and local eruptive centers (Fig. 2;

Accordi et al., 1966; Angelucci et al., 1974; Alberti et al., 1975; Pasquarè et al., 1985; Boari et al., 2009; Centamore et al., 2010 and references therein).

The pre-volcanic substrate is composed of shallow-water carbonates, dominated by inner platform to rim facies during the Mesozoic and by temperate discontinuous ramp deposits during the Cenozoic (e.g., Centamore et al., 2007, 2010; Consorti et al., 2017; Romano et al., 2019). In particular, the marly Orbitolina level (Sirna, 1963) constitutes a regional marker horizon used to subdivide the Cretaceous succession. At the top of the carbonate succession, middle to late Miocene syn-orogenic siliciclastic rocks occur at the footwall of thrust faults related to the (E)NE-verging Apennine orogeny (Angelucci, 1966b; Cosentino et al., 2002; Sani et al., 2004). In particular, at least four orogenic lithostratigraphic units are distinguished: i) the late Miocene Falvaterra Chaotic complex (Centamore et al., 2007; also known as 'Argille Caotiche'; Angelucci et al., 1963), ii) the late Tortonian flysch of the Frosinone Formation (Centamore et al., 2007, 2010), iii) the Messinian pp. Torrice Sandstone Formation (piggyback basin deposits, Cipollari & Cosentino, 1995); iv) late Miocene to early Pliocene conglomerates (Alberti et al., 1975). The latter unit occurs at the front of the chain as thrust-top deposits (e.g., Angelucci 1966a; Cipollari & Cosentino, 1995), and at the footwall of backthrusts (e.g., Accordi et al., 1966; Angelucci et al., 1974; Cosentino et al., 2002; Parotto & Tallini, 2013). Early to late Pleistocene slope, river and lacustrine deposits are preserved within depressions determined by high-angle NW-, ENE- and (N)NE-striking normal faults that dissected the inherited fold-and-thrust fabric, influencing the distribution of karst form and the fluid circulation. While the main hydrogeologic unit has a piezometric head below 125 m a.s.l. (Boni et al., 1980), minor aquifers are suspended above it at the intersection between normal faults and the Orbitolina level. Further to the south, upwelling S-rich fluids interact with cold karst water generating sources that can

reach temperatures up to 24ºC (10ºC higher than average local surface temperature; Boni et al., 1980; Capelli et al., 2012).

2.1 Volcanic deposits of the northern Volsci Range

Volcanic terrains in the study area comprise (see also supplementary material in Data in Brief): i) distal pyroclastic deposits from the nearby Colli Albani potassic volcano, recognized within middle-lower Quaternary continental successions in the Latin Valley, in the Pontina Plain and locally in the VR intermontane depressions; ii) locally sourced eruptive products, for the most part occurring in the northern VR. The latter mostly consist of pyroclastic products of both magmatic and phreatomagmatic origin, respectively associated with monogenetic scoria cones and tuff rings, and subordinate lavas. In the previous literature, they have been attributed to the Middle Latin Valley Volcanic Field (e.g., Accordi et al., 1966; Angelucci et al., 1974; Alberti et al., 1975; Boari et al., 2009; Centamore et al., 2010), also known (improperly) as Monti Ernici Volcanoes.

Reconsidering the whole areal distribution of the monogenetic vents between the Pontina Plain, the VR and the Sacco Valley, with respect to the geographic and historical pertinence of ancient populations, here we propose the term Volsci Volcanic Field (VVF). The VVF rocks are scattered over an area of ~500 km^2, covering an area of ~120 km^2 (Angelucci et al., 1974). Based on available geochronological data (Boari et al., 2009; Centamore et al., 2010 and references therein), the VVF volcanic activity spanned the 760-230 ka interval, with an acme at 420-350 ka). Despite the broadly similar time span of activity, the VVF features remarkable peculiarities with respect to the other potassic volcanic districts of central Italy: i) the small volume (a few km^3 vs. hundreds of km^3) of total erupted products; ii) the low intensity and magnitude of eruptive events (essentially Hawaiian-Strombolian and phreatomagmatic vs. Plinian and caldera-

forming activities); iii) the primitive to poorly differentiated character of rock-types (as described in the following).

Based on isotope geochemical affinity (e.g., $^{143}Nd/^{144}Nd$ vs $^{87}Sr/^{86}Sr$), Peccerillo (2005) grouped the VVF volcanics within the Ernici-Roccamonfina Volcanic Province, distinct from the Roman and Campanian ones. Overall, geochemical and petrological data (Angelucci et al., 1974; Boari and Conticelli, 2007; Frezzotti et al., 2007; Boari et al., 2009; Centamore et al., 2010) indicate the eruption of poorly to slightly differentiated potassic magmas, ranging from K-basalts to shoshonites and phonotephrites in the TAS diagram. The concomitant eruption of high-K, Lct- and low-K, Plg-bearing primitive magmas during the VVF activity may have implications for the mantle source and related slab-tear window and magma ascent conditions. The absence of a main volcanic edifice and of a large, shallow-level magma reservoir would be consistent with the rapid ascent of primitive magmas from the mantle source, with limited pre-eruptive stationing and differentiation (Boari et al., 2009; Centamore et al., 2010). The parental VVF magmas might have been generated from a heterogeneous subcontinental lithospheric mantle source resulting from metasomatic processes, although the timing of the metasomatizing event(s) and the geometry of the heterogeneity are still matter of debate (e.g., Boari et al., 2009; Gaeta et al., 2016; Koornneef et al., 2019).

3. Materials and methods

3.1. Field analyses

This study is based on a new structural-geological survey of the carbonate substrate and volcanic occurrences, which integrates previous work (e.g., Geological Map of Italy; Accordi et al. 1966; Alberti et al., 1975; Centamore et al., 2010, and references therein), aiming at re-

defining the stratigraphic and structural architecture of the substrate, and identifying the relic morphologies and eruptive products of the VVF rooted centers. Structural elements (i.e., faults, fractures) have been measured at key localities and plotted by means of TectonicsFP software with lower-hemisphere projections and rose diagrams. The morpho-structural interpretation is also based on the analysis of the orientation of river and valley segments and relieves characterized by break-in-slopes with dip >20% (on Google Earth software), which allows to qualitatively attribute these forms to near-surface fault traces cutting through volcanic deposits. Inferences on sub-surface deep geometry are supported by available seismic reflection lines and wells in the Middle Latin Valley from a public data set (ViDEPI Project; www.videpi.com). The data set has been calibrated with deep well logs and integrated with the reappraisal and critical review of a large amount of literature data. Fault trace maps, created from the geological map and seismic line-based maps, were used to estimate fault segment orientation using FracPaQ (Healy et al., 2016).

VVF volcanic deposits, with special focus on phreatomagmatic products from carbonate-seated maar-diatremes, were characterized through the detailed definition of field characteristics (e.g., deposit textures, grain size, componentry, lithofacies architecture), by means of layer-by- layer thickness measurements and facies analysis, in light of well-established interpretive criteria of eruption and emplacement processes (e.g., Németh et al., 2001). In some cases, we estimated the order of magnitude of the erupted volume of individual centers, based on the thicknesses and areal distributions of the exposed deposits, also taking into account local topographic control and adding further 50% to account for fine-ash loss in the atmosphere (e.g.; Ernst et al., 1996). Thus, the volumes obtained here are minimum estimates based on the ejecta ring (cf. Blaikie et al., 2015), as uncertainty of intra-crater and diatreme fills and erosion loss

prevent a reliable determination of total erupted magma volume (lithic-free dense rock equivalent, DRE).

3.2. Laboratory analyses

Laboratory analyses comprise the determination of componentry and morphoscopic characteristics of phreatomagmatic products associated with maar-diatremes, including observations on the juvenile scoria fraction and on accessory and accidental lithic inclusions. Preliminary qualitative determinations were based on thin sections at the optical microscope from samples collected at twenty-eight localities from different stratigraphic units (Table S1). Moreover, sixty-four thin sections were analyzed to anchor the bio- and litho-stratigraphic content of accidental pyroclasts embedded in the phreatomagmatic deposits (i.e., essentially fossil-bearing carbonate ejecta with different degrees of thermal interaction) to the pin stratigraphic columns of the VR (Chiocchini & Mancinelli, 1977; Chiocchini et al., 2008) to identify their stratigraphic provenance.

Quantitative component determinations of the erupted juvenile and lithic proportions and textural analysis of carbonate lithics and cored scoria clasts were carried out to gather information on pre- to syn-eruptive lithic entrainment and fragmentation vs. recycling processes. In this regard, thirty pictures of polished rock slabs were selected out of twenty-three samples representative of the main eruptive centers and then analyzed by using the JMicroVision software for image analysis (Roduit, 2008). Nearly 500 measurements per sample were taken on a standard grid from pictures covering an arbitrarily chosen (3x3 cm) area. The relative abundances of eight component classes were thus determined, i.e.: ash matrix, juvenile fragments, carbonate lithics (with no evidence of thermal effects), thermally altered and thermo-

metamorphosed carbonate lithics, free crystals, accretionary lapilli, accessory pyroclastic fragments, holocrystalline inclusions.

In addition, we collected hand samples from eight selected outcrops of lithified tuffs rich in carbonate lithics (*peperino*-type, see definition in Results below). For each sample, five differently oriented polished slabs, up to 10 cm across, and thin sections were analyzed. Specifically, on slab surfaces, the clast size (long axis in mm), degree of roundness and degree of whiteness of nearly 750 carbonate lithics were measured. Lithic roundness was measured according to the 1-6 scale of Powers (1953), being 1 very angular and 6 well rounded. In our point of view, due to the limited subaerial lateral transport, clast angularity depends straightforward on the fragmentation and abrasion history (due to multiple explosions and recycling) during ascent in the feeder diatreme. The different degree of whiteness of accidental carbonate lithics, which is usually stronger from the edge to the core, is considered as representative of thermal alteration or thermo-metamorphism. Thus, to quantify the degree of thermal alteration, for each single carbonate lithic, the degree of surface whiteness was evaluated visually according to a chromatic scale from 0% (corresponding to the unaltered, starting rock colour) to 100% (pure white), as representative of progressively longer and/or intense thermal effects. All measurements were repeated twice. To track the stratigraphic provenance (and the depth of entrainment), we bear on micropaleontological thin section analyses of clasts where the original biostratigraphic assemblage was not obliterated by pervasive thermal alteration. In addition, to infer thermal conditions of wall-rock entrainment during diatreme processes, we analyzed the textural features of cored lapilli, following the approach of Sottili et al. (2009, 2010).

4. Results

4.1. Volsci Range stratigraphic and structural constraints

A new field survey is summarized in the geological sketch map of Figure 2, where the fault and volcanic occurrence patterns highlight the carbonate and foredeep orogenic structure and their control on the location and activity styles of VVF eruptive centers. In addition, detailed structural maps are shown in the Data in Brief, along with the description of relic volcanic morphologies and deposit characteristics.

In Figure 3, the stratigraphic frame of the VR pre-volcanic substrate is anchored to the exposed carbonate aquifer stratigraphic sections, based on the analysis of the lithic inclusions in the VVF pyroclastic units (Table S1). Along the southern slope of the Semprevisa Mt., the reference Cretaceous carbonate succession (Fig. 4; broadly corresponding to the CMS and PUO formations; Centamore et al., 2010) comprises, from bottom up: i) wackestone to mudstone, alternated to greenish marly levels with Salpingoporella dinarica; ii) a key marker horizon, the *Orbitolina* level, i.e. a 1 m-thick, beige to bluish shaly marl with Charophyta that contains Early Cretaceous pebbles; iii) upper Aptian-lower Cenomanian ostracoda- and miliolid-bearing laminated limestones, including a few tens of meters thick dolostones, and karstified wakestone to packstone limestones, directly overlapping the *Orbitolina* level with a sharp unconformity, occurring on mountain plateaus and karstic terraces formed at the expense of strongly fractured limestones; iv) well-bedded Cenomanian Alveolinid- and Nezzazzatid-bearing limestones, usually cropping out on rounded reliefs. The texture of the *Orbitolina* level changes to the east (e.g., at Patrica), with implications discussed below. Here, a series of breccias and calcirudites

with thin green pelite intercalations (broadly coeval to ii and iii) occurs and is characterized at the base by ostracoda- and miliolidae-bearing laminated limestone (affected by incipient bauxitic facies) with upper Aptian to lower Cenomanian limestone benthic assemblages.

Structurally, the VR is here subdivided into three major thrust sheets, based on major tectonic contacts and internal stratigraphic pertinence (from the lowest to the highest): i) the Ernici Unit (EU), characterized by a doubled succession of siliciclastic late Miocene foredeep deposits lying on Upper Cretaceous to Miocene carbonates; ii) the Lower Volsci Unit (LVU), constituted by Jurassic to Cenozoic carbonates; and iii) the Upper Volsci Unit (UVU), which is preserved at the Caccume Mt., Siserno Mt. and Colle Cantocchio klippen and within the Carpineto Romano tectonic window (Fig. 2).

The UVU marl-and-clay-rich matrix bears heterometric rounded to sigmoidal clasts of: glauconitic calcarenite with bryozoa (corresponding to early Miocene lithotypes; Angelucci et al., 1963), white-mica-bearing sandstone, brownish folded calcareous sandstone, green sandstone, veined and fracture calcareous marls (corresponding to the Paleocene 'Pietra paesina' lithotype; Civitelli et al., 1970), pinkish marl (corresponding to the Scaglia facies-type of Paleocene-Eocene pp.; Angelucci et al., 1963), *Orbulina* Marl lenses of late (?) Serravallian-Tortonian p.p. age (Centamore et al., 2010).

The EU-LVU contact is masked in the northern VR, although it is evidenced by a series of imbricated, overturned Cretaceous to Cenozoic carbonate layers (i.e., NW of Morolo). Notably, the top of LVU is characterized by encrusted and lineated Late Cretaceous carbonates, overthrusted by the Chaotic complex towards the East (Fig. 4), which are cross-cut by high-angle, ENE-trending en-echelon fracture zones, constituted by NNW-striking open fractures. Further, the northern VR is crossed by a series of SW-verging backthrusts, the largest one being

the Montelanico-Carpineto backthrust. On its hanging wall, we identify a frontal subunit that occurs as a large-scale antiform, while further to the east it is defined by a synform. The two folds are separated by a series of NNW-striking tear faults with inferred right-lateral kinematics (Fig. 4). The resulting fold-and-thrust structure defines a N-trending flank of a salient, later crosscut by a system of conjugated normal faults onto which most of the VVF monogenetic eruptive centers are seated (Figs. 2, 4).

To the southwest, step-wise segments of the normal faults bound the Pontina Plain. Further to the northeast, domino-like blocks are bounded by 2-3 km spaced faults, having about 0.5 km offset each. Along the chief ridge of the VR (mountain backbone), the largest Quaternary normal fault in the study area (here named as the Semprevisa Fault; Figs. 2, 4), occurs as a fault system characterized by lateral strike deviation and offset reduction to a few hundreds of meters at its tips (Fig. 2). In particular, at Maenza, the Semprevisa Fault connects with the asymmetric graben structure of the middle Amaseno Valley. Antithetic normal faults bound the north-eastern VR with segments shorter than 5 km (i.e., NE Volsci Fault system, Fig. 2, 4).

4.2. Field aspects of VVF eruptive centers

Here we report on volcanic terrains exposed in the VR study area, with focus on the products of local monogenetic centers of the VVF, setting the groundwork for ongoing volcanological, petrological and geochronological studies. In the Data in Brief, we show the outlined volcanic stratigraphy at key localities. In some cases, we integrate the available data on known eruptive centers (cf. Centamore et al. 2010 and references therein); in a few cases, we describe field aspects of deposits and relic morphologies of newly identified eruptive centers. Notably, the original depositional features, thickness and internal stratigraphy of volcanic units are highly fragmentary, due to their intrinsic limited areal extent and spot-like distribution, as

well as their scarce preservation. Field-based stratigraphic correlations are thus challenging and uncertain.

The areal distribution of volcanic terrains is reported in Figure 2. Below we do not further consider the local occurrences of volcaniclastic deposits (mostly reworked) from distal sources, essentially attributed to major explosive eruptions from the Colli Albani Volcanic District, based on their peculiar lithostratigraphic features (i.e. field texture, grain size and componentry; e.g., Freda et al., 1997, 2011; Palladino et al., 2001; Giordano et al., 2002; cf. Data in Brief). Distal pyroclastic deposits are mostly found in the western part of the study area, along the VR foothill and in intermontane basins (e.g., Montelanico, Norma, Valvisciolo creek, Roccagorga, Crocemoschitto; Fig. 2), while along the mountain backbone they mostly occur as pedogenized terrains within karst depressions (e.g. Semprevisa Mt. northern slope).

Based on lithofacies assemblages that show evidence of proximal, near-vent setting (such as coarse grain size, occurrence of ballistic bombs with impact sags, pyroclastic surge sandwave bedforms) and related relic morphologies (crater rims, volcanic edifices), fieldwork allowed us to distinguish the different eruptive source areas, including either isolated eruptive centers or clusters of coalescent vents (Fig. 5; Table S1). We group eruptive centers in two main geomorphic settings: the Sacco River valley (part of the Middle Latin Valley) and the Volsci mountain range (including backbone and foothill), broadly corresponding to the Frosinone foredeep and the VR carbonate belt structural domains, respectively. Based on well-established textural features and associated relic morphologies (e.g., scoria/spatter cones and tuff rings), we distinguish three main types of eruptive products: i) lava occurrences (lava flows and occasional dykes); ii) scoria and spatter fall deposits from Hawaiian-Strombolian activities; iii) phreatomagmatic deposits, related to maar-diatreme systems and related tuff rings (e.g.; White &

Ross, 2011; Valentine et al., 2015 and references therein). In some VVF centers, magmatic and phreatomagmatic products were erupted together (Centamore et al., 2010).

In the VR domain, we recognized at least ten eruptive centers, rooted in the Meso-Cenozoic carbonate substrate (Fig. 2, 5). Their original morphologies are largely obliterated, so this identification is essentially based on deposit characteristics. In Table S1, for each sampled source area, we summarize the principal field aspects of deposits and present-day morphologies. In particular, phreatomagmatic deposits comprise planar to cross-bedded, accretionary-lapilli bearing, ash deposits from base surges, alternating with thin, scoria lapilli fallout layers. The most typical lithology in the eruptive centers of the VR mountain setting (e.g., Fosso di Monteacuto, Patrica, Patrica NE, Villa S. Stefano) is represented by *peperino*-type pyroclastic current deposits. The Italian term *peperino* (cf. Peperino di Marino from Colli Albani; Marra et al., 2003) refers to massive to faintly stratified deposits with strongly lithified grey ash matrix, enclosing dark clasts of scoria lapilli, lava and/or holocrystalline mafic inclusions, and whitish clasts of carbonate lithics, as well as leucite (often turned to analcime), clinopyroxene and dark mica free crystals, and occasional accretionary lapilli. Strongly lithified, granular massive beds made up of well-sorted, fine scoria lapilli, with pervasive interstitial calcite are also present. This lithofacies thickens up to a few tens of meters where channeled in topographic lows. The VVF phreatomagmatic surge deposits show evidence of low to moderate emplacement temperatures, such as the occurrence of plant remains, accretionary lapilli, occasional charcoal, vent-derived carbonate inclusions with variable degree of whiteness and cored lapilli (see below).

The patchy distribution of the present-day exposures and the scarce degree of preservation due to erosion (especially in the VR rugged mountain context) prevents a reliable reconstruction of the volume of erupted products based on isopach maps. However, a broad

estimate indicates that monogenetic centers range in the order of 0.001-0.01 km^3 (e.g., Sermoneta, Valvisciolo, Fosso di Monteacuto, Prossedi, Pisterzo) to 0.01-0.1 km^3 (e.g., Patrica centers and Villa S. Stefano in the VR backbone, along with individual centers in the Ceccano and Pofi source areas; e.g., Fiano, Colle La Grotta, Colle Marte; Centamore et al., 2010).

4.3. Volcano-tectonic relationships of VVF eruptive centers

The distribution pattern of the rooted eruptive centers of the VVF highlight alignments and/or belts of clustered monogenetic centers (scoria/spatter cones, lava occurrences, maar-diatremes). We define three orders of volcano-tectonic trends, based on the length scale, relationships with fault segments and other morphotectonic indicators.

Two principal (first order) structural trends, striking NNE and ENE, respectively (Figs. 5, 6) are considered the surface expression of high-angle lithospheric faults (e.g., Rosenbaum et al., 2008) that cross the Latin Valley foredeep and the VR fold-and-thrust belt domains. The NNE-trend (between Tecchiena and Pisterzo; partly identified by Acocella et al., 1996 and Acocella and Funiciello, 2006), includes at least seven eruptive centers, spaced 2-4 km from each other, within an area 23 km long and 2-3 km wide. The ENE-trend is defined by an elongate zone that extends at least 25 km in length between Pofi and Roccagorga-Maenza, and about 6-7 km in width. Limitedly to the Sacco valley, this trend is represented by the Ceccano normal fault (recognizable for a length of 13 km), which is mostly inferred by morphologic evidence and limited fault exposure within carbonate terrains near Ceccano. This fault consists of step like dextral en-echelon segments, possibly reflecting strike slip kinematics. We note that several centers of the Ceccano and Pofi areas sit on the hanging wall, while the Arnara center lays on the footwall.

The second-order trends (Figs. 5, 6) are defined by the eruptive centers aligned along NW-, NE-, N-trending structures, associated with major horst and graben-bounding fault systems (up to 7-10 km long fault segments, with displacements up to 0.7-1 km) that cross-cut the VR fold-and-thrust belt carbonates. In these cases, eruptive centers are located right along (or within 1 km from) recognized fault traces. For instance, the (W)NW-striking Semprevisa Fault and the NW-striking, SW-dipping, Giuliano di Roma normal fault (4.5 km long), are associated with sources of effusive, strombolian and phreatomagmatic activities (i.e., Valvisciolo, Maenza, Roccagorga located at the hanging wall of the first, and Giuliano di Roma and Villa S. Stefano centers at the hanging wall of the second). Moreover, some eruptive centers of the Ceccano cluster (e.g., from La Badia to Colle Vento) occur at the hanging wall of the NE-dipping fault bounding VR.

Furthermore, NNW- and (E)NE-striking third-order structures (Fig. 6) are suggested by break-in-slope (>20%) occurrences along the Sacco River valley, which share a similar orientation with outcropping faults, valley and river segments. We qualitatively attribute these forms to near-surface fault traces. These minor structures are disposed en-echelon at the hanging wall of the Ceccano Fault and show to have crosscut products and relic morphologies of eruptive centers. Also at Patrica, nearby, the orientation of the fractures affecting phreatomagmatic deposits is compatible with the second-order normal faults, indicating post-eruptive NW-striking neotectonic fractures.

4.4. Componentry of VVF phreatomagmatic deposits

Component proportions from representative slab samples of phreatomagmatic deposits are reported in Table S2. The component data set allows us to roughly estimate the relative proportions of juvenile vs. lithic material, along with carbonate vs. volcanic country rocks (in the

fine lapilli fraction). Within volcanic ejecta, which include both juvenile and accessory components (not always easily distinguishable in phreatomagmatic eruption products), the dominant juvenile component consists of moderately vesicular, variably porphyritic scoria fragments (usually from fine- to coarse lapilli- sized) with microcrystalline groundmass and clinopyroxene, leucite, dark mica (and occasional olivine and plagioclase) phenocrysts. The same mineral phases are also present as free crystals. In places, cored scoria lapilli and accretionary lapilli also occur. The ash matrix (in the <1mm fraction) varies between 40 and 88 vol%. Volcanic fragments often contain accessory tuffs and holocrystalline granular aggregates. Among the monogenetic phreatomagmatic centers of the VR mountain backbone, the deposits of Fosso di Monteacuto contain the highest proportion of both accidental carbonate (up to 33 vol%, including thermally affected) and accessory (mostly tuffs; ~11 vol%) lithics. In particular, outcrops at Patrica, Valvisciolo and Prossedi show wide component heterogeneity from sample to sample from different surge units. Lithological associations and comminuted grain size point to diatreme-derived clasts, rather than locally collected clasts from the ground surface.

4.5. Cored juvenile clasts

In some cases, the VVF eruption products show occurrences of cored juvenile clasts, usually millimetre-sized (up to 1 cm long axis). These consist of dark-rounded to reddish-asymmetric, shells of juvenile scoria material surrounding grains of different lithology. On the basis of Colli Albani examples (Sottili et al., 2009, 2010), two end-member types are recognized in the VVF: i) dominant, rounded clasts made up of a relatively thin coating of juvenile material around a single lithic core, and ii) occasional, irregular scoria clasts including one or multiple lithic fragments. Slab observation (Fig. 7) reveals that the enclosing shells consist of up to three, variably porphyritic and vesicular scoriaceous layers, which enclose either single or multiple

accessory (e.g., lava and tuff fragments, individual leucite, clinopyroxene, olivine and dark mica xenocrysts) or, quite subordinately, accidental (carbonate) grains. From case to case, the average thickness of the shell (Δr) vs. the radius of the core (a) displays specific trends related to the different nature of the core that will be discussed in Section 5 in terms of thermal gradients (following the approach of Sottili et al., 2009).

4.6. Micropaleontology of carbonate lithics

An amount of 733 carbonate lithics was collected from several phreatomagmatic surge units at different sites (Patrica-Supino area, Fosso di Monteacuto, Prossedi, Pisterzo, Villa S. Stefano, Valvisciolo; Figs. 7). Of these, carbonate clasts with evidence of no (or very low) thermal interaction (expressed by whiteness <7%) were selected for micropaleontological determinations. The biostratigraphic belonging of fossil-bearing carbonate lithics is reported in Fig. 3, while detailed determinations are shown in the Data in Brief (Fig. S7; Table S3). Most carbonate lithics, representative of Upper Cretaceous aquifers, show grainstone to wackestone textures and belong either to the Ostracoda and miliolidae laminated limestone unit or to the Alveolinid and Nezzazzatid limestone unit (sect. 4.1). Just a few samples are representative of: 1) Lower Cretaceous limestone and dolostone unit; and 2) Campanian part of the Hippuritid and Radiolitid limestone unit (see Sect. 4.1). The Patrica locality provides the only occurrence of Berriasian-Aptian *Salpingoporrella* association. On the other hand, the most frequent foraminifer associations at Patrica village, Fosso di Monteacuto and Valvisciolo consist of *Nezzazzata* and of some specimens of *Sellialveolina*, both Cenomanian in age (Fig. 3). At Patrica (Pietrapizzuta locality, see Data in Brief), *Peneroplis parvus* De Castro was found, attributing a Cenomanian age, that is typical of suspended aquifers (Fig. 4). On the contrary, wackestone-packstone

limestones with *Thaumatoporella*, *Scandonea mediterranea* De Castro and *Accordiella conica* (Farinacci) are Coniacian-Santonian in age and less common. Finally, the lithics collected from the Ceccano centers, are mostly constituted by Miocene calcarenites with operculiniform Foraminifera and are possibly representative of shallower magma-water interaction levels.

4.7. Texture of carbonate lithics

Concerning size-texture relationships, fine- to coarse carbonate lithic lapilli vary from very angular to well-rounded (1 to 6 according to the scale of Powers, 1953). They occur as virtually undisturbed fossil-bearing limestone clasts or as clasts with variable degrees of whiteness toward their edges, due to thermal effects at the depth of magma-wall rock interaction, resulting in re-crystallized marble-type texture to variable degrees of whiteness (Fig. 7). In some cases, whitened edges of carbonate fragments occur as concentric haloes with variable degrees of whiteness. In some examples, this zoned fabric is cut sharply by a new fracture onto which a new whitened edge develops, suggesting a multistage sub-surface fragmentation and transport history (i.e., a fragmentation event, followed by rounding and magma thermal effects, then a new fragmentation event, creating new surfaces exposed to magma thermal effects). Fig. 7 illustrates the relationships among size, degree of whiteness and roundness of carbonate clasts. Overall, two clusters are distinguished: a “cold” cluster, defined by null whiteness values (except for one sample with 7%), which is virtually unaffected by thermal alteration, and a “hot” cluster, defined by moderate to high (19-100%) whiteness values, related to prolonged and/or intense thermal interaction (or even thermo-metamorphism). The first group shows increasing rounding with fining grain size, essentially due to progressive attrition during diatreme transport. In the second group, samples from individual eruptive centers show specific trends of increasing whiteness

with decreasing clast size. For instance, at Fosso di Monteacuto, clasts with a given size show a scatter in the degree of whiteness, indicating that the degree of thermal interaction, beyond a mere function of clast size in an outside-in alteration process, is actually related to more or less intense thermal alteration (or even thermo-metamorphism) related to different interaction depths along the diatreme. Also, for a given clast size, a higher degree of rounding would imply a more significant role of progressive recycling vs. explosive phreatomagmatic fragmentation in the diatreme system.

5. Discussion

In the following, we discuss the structural geometry of the VR and its relationship with the VVF activity, with special reference to maar-diatreme processes.

5.1. Structure of the Volsci Range

The deep structure of the VR and the adjoining Latin Valley and Pontina Plain is so far poorly constrained, due to the scarcity of available wells and seismic lines, and the uncertain age of the different syn-orogenic deposits. Here, we present two geological cross-sections in light of new field structural data and a reinterpretation of available seismic lines (Fig. 8), aiming at providing a structural frame for the possible sites of magma-carbonate interaction.

In the mountain backbone, the cross-section is constrained by new field data, while the subsurface structural setting of the Sacco Valley is based on available geological maps (Accordi et al., 1966; Centamore et al., 2010) and subsurface data (www.videpi.com). The interpretation of the seismic line Fr306-80 in Fig. 8, acquired between our geological cross-sections, is considered representative of the tectonic setting at depth (besides minor differences in the pattern of Quaternary normal faults between the northern and southern part of the Latin Valley),

allowing us to constrain the top of the carbonate substrate from the near-surface down to ca. 1 km depth (Fig. 9). The thickness of the syn-orogenic units varies depending on the fold-and-thrust belt structure, being the siliciclastic deposits thicker to the south (up to 1.5 km) and thinner to the north (usually limited to 0.7 km). According to previous works, the LVU carbonates constitute one or multiple thrust sheets that, together with the overlaying siliciclastic unit, overthrust the Frosinone Fm. In particular, the Chaotic complex was found to occur between the late Tortonian Frosinone Fm and LVU, possibly implying that gravitational sliding into the foredeep occurred during early Messinian after its tectonic emplacement on top of the VR. Thus, during late Miocene to early Pliocene, the VR carbonate successions were progressively involved into crustal shortening: thrust 1 allowed the emplacement of the UVU; thrust 2 accommodated the doubling of the Upper Cretaceous to upper Miocene sedimentary rocks within the Frosinone foredeep domain, which hosted the buried and pressurized reservoirs later involved in phreatomagmatism; thrusts 3 is mostly represented by backthrusts that crosscut the previous 1-2 fabric. According to Acocella et al. (1996), a thin thrust sheet of Upper Cretaceous carbonates and flysch units is juxtaposed on the same flysch north of Tecchiena. This thrust represents the front of Thrust 2 (Figs. 8, 9; corresponding to ϕ1 of Sani et al., 2004), which was crosscut by a NW-striking conjugated normal faults. The cut-off relationships do not allow the exposure of thrust 2; however, both morphologic and structural evidence (e.g., at Patrica) suggests that normal faults are prominently shaping the VR north-eastern flank (Figs. 2, 4). Therefore, this is due to the second thrusting phase of the LVU over the EU during the deposition of the early Messinian Torrice Fm (Figs. 3, 8). Similar to what reported elsewhere in the Apennines (e.g., Cardello & Doglioni, 2015; Fabbi & Smeraglia, 2019), backthrusts occur also in the VR.

Crosscutting relationships and geomorphic evidence indicate that normal faults are superimposed to the thrust system, creating a horst and graben structure tied to the Tyrrhenian margin backarc extension. Furthermore, Quaternary normal fault activity evolves into a mainly NW-oriented horst- and-graben structure that is associated with ENE- and (N)NE-striking high-angle faults with lateral kinematics. A major horst occurs between Maenza and Patrica, while the Middle Latin Valley graben involves part of the Frosinone foredeep domain, which is further dissected into minor blocks (Fig. 9). Differently by older interpretations envisaging minor normal faults, in our reconstruction, this graben is bounded to the southwest by an antithetic step-wise set of normal faults, along which monogenetic centers were located (i.e., Patrica-Supino, as well as Selva dei Muli and Tecchiena magmatic centers that occur near the intersection between NE- and NW-striking normal faults). As already recognized by Acocella et al. (1996), smaller horst- and graben-structures are related to the conjugated Giuliano di Roma and frontal normal faults, respectively associated with the Giuliano di Roma-Villa S. Stefano centers to the south-western side and with the Ceccano centers to the north-eastern side (Fig. 9). However, seismic lines and available time maps do not support the existence of a previously published major N-S fault in the Latin Valley (Acocella et al., 1996). Rather, limitedly to the VR, we recognize the N-trending flank of salient close to Prossedi (Figs. 2, 4), which set up in the Messinian according to Acocella et al. (1996). We consider this element separated in space and time from the NNE-trending alignment of middle Pleistocene rooted centers in the Latin Valley that, together with the ENE- and NW-trending alignments, clearly drove the emplacement of dykes along high-angle faults. In agreement with Ruch et al. (2016), we found that the reactivation of pre-existing fractures and faults is a fundamental for rifting mechanisms and occasionally guides dyke emplacements along the extensional Tyrrhenian margin.

5.2. Volcano-tectonics of the Volsci Volcanic Field

Volcanic fields often comprise several tens of individual monogenetic centers, which may include magmatic and phreatomagmatic centers arranged in clusters and/or alignments that provide information on the magma feeder system and regional tectonic lineaments (e.g., Lorenz, 2003; Mazzarini & D'Orazio, 2003; Sottili et al., 2012; Le Corvec et al., 2013; Tadini et al., 2014, and references therein). The observed distribution patterns of VVF eruptive centers are strictly linked to structural patterns at different scales (as also reported elsewhere, e.g., Tadini et al., 2014; Trippanera et al., 2015), thus allowing us to draw some general implications on the relationship among location and styles of volcanism and tectonics. Although the NNE-trend does not show clear near-surface fault evidence, it could be associated with deep-seated (mainly extensional) faults. We suggest that the NNE-trending eruptive cluster may be linked to the reactivation of a inherited high-angle Mesozoic rift fault (subparallel and associated with the major Ancona-Anzio and Ortona-Roccamonfina tectonic lines). Differently, the ENE-trend is clearly associated with the Ceccano Fault and the major middle Amaseno Valley faults, as part of a larger dextral wrench zone cutting across the VR, which could be tentatively related to subduction kinematics. In particular, the ENE-trend can be interpreted as the result of a lateral slab-tear due to the differential retreat of two portions of the subducting Adriatic slab (cf. Central Apennine slab window; Rosenbaum et al., 2008). Thus, in light of the local geodynamic setting (e.g., Doglioni, 1991; D'Orazio et al., 2007; Rosenbaum & Piana Agostinetti, 2015), first-order alignments of VVF eruptive centers may represent deep-seated structures that controlled magma ascent at crustal levels (NNE-trend) or even at higher depth within an asthenospheric shear zone in the hanging wall of the segmented subducting slab (ENE-trend). Second-order alignments

represent the expression of near-surface fault segments that laterally branch off the first-order trends, thus controlling the location of feeder conduits and diatremes.

At shallow crustal levels, the carbonate wall rock architecture controlled the path of feeder dykes and vent distribution, as well as the styles of volcanic activity (i.e. magmatic vs. phreatomagmatic). Indeed, the eruption of poorly differentiated magmas through the thick carbonate-rich orogenic structure in the VR backbone setting (hosting a major water table), often acquired a phreatomagmatic character due to magma-water explosive interaction. Indeed, the levels of interaction can be guided by the inherited geological structures (i.e., rock fabric, aquifer permeability, faults and fold hinges) and/or be associated with active faulting (Valentine & Cortés, 2013; Valentine et al., 2017). In this regard, the VR tectonic displacement set multiple depth levels of magma-water interaction, thus controlling the explosion loci and likely resulting in complex 3-D maar-diatreme geometries (Fig. 9; see also section 5.3).

In particular, the distribution pattern of VVF maar-diatremes is tightly associated with major high-angle fault zones that favored magma-groundwater interaction by connecting stratigraphic levels characterized by enhanced fluid transmissivity and acted as feeder conduits to the surface. The VVF phreatomagmatic centers commonly occur at the intersection between differently oriented faults (Fig. 5) or, subordinately, within fold hinges, as in the case of the Fosso di Monteacuto fold hinge (Fig. 9), that was also affected by a NW-striking normal fault with a modest displacement (<50m). The associated antiform is the southeastern continuation of a major backthrust (i.e., Montelanico-Carpineto Backthrust; Fig. 2), which allowed the doubling of the UK_L succession that later interacted with ascending magmas during phreatomagmatic eruptions. Similarly, the Patrica-Supino centers are associated with conjugated normal faults. Within the Sacco Valley, magmatic occurrences (lava and scoria cones) are directly related to

middle Latin Valley graben structures (i.e., Ceccano Fault and NE Volsci Fault), while the phreatomagmatic centers are essentially associated with carbonate substrate highs (Figs. 2, 5, 8).

5.3. Diatreme processes

Observations on carbonate lithic inclusions, in light of seismic lines in the Latin Valley and new field data in the VR, provide constraints to the depth of explosive magma-aquifer interaction at carbonate-seated maar-diatremes, indicating the litho-stratigraphic and structural control on explosion loci (Figs. 3, 8, 9). The above-reported data on carbonate lithics show that they are mostly representative of the lower part of the UK succession (i.e., late Aptian-early Cenomanian ostracoda and Miliolid laminated limestone and dolostones). According to our reconstruction, UK can be structurally repeated up to three-four times, and thus the Orbitolina level may occur at multiple depths, acting as regional karstic aquiclude, décollement level for very thin-skinned thrust sheets, and controlling the sites of explosive magma-water interaction. In the carbonate aquifer, the Orbitolina level may favor the explosive fragmentation of the UK rocks even beneath the piezometric head, possibly due to pressurized conditions. Based on field appearance, the lower part of UK succession is much more karstified than the overlying units, powering fluid circulation. While primary porosity was likely enhanced by dolomitization-related brecciation during diagenesis, secondary porosity may be ascribed to fracturing and multiple karst events that in the late Cretaceous and late Neogene to Quaternary may have increased the capacity of fluid circulation in the reservoir.

On these grounds, magma-aquifer interaction is broadly inferred to have occurred near-surface (i.e., <500 m below the present day average countryside plan) and/or at deeper levels (i.e., -800 to -2300 m below the present day average countryside plan; Fig. 9). For instance,

among the study cases, biostratigraphic dating from samples collected at Patrica near-vent area, indicate the preferential entrainment of the Albian-Cenomanian limestones, which may have occurred even twice, respectively at depths of about 2000-2300 m and/or 800-1000 m below the present topography (Fig. 9), related to the tectonic repetition of UK formations due to thrusting and normal faulting.

In light of partially exposed diatreme examples (e.g.; Re et al., 2016 and reference therein) and experimental evidence (e.g.; Graettinger et al., 2014), the subsurface geometry may be repeatedly modified by dynamic processes, such as changes in magma supply rate, magmatic-phreatomagmatic transitions, deepening of the fragmentation levels, in the course of an eruption. Thus, earlier emplaced dikes and breccia domains of fragmented magma and wall-rocks may be removed and/or overprinted to a variable extent by multiple magma-water explosive interactions at multiple depths. For example, at Patrica (Fig. 9), early/deep-seated magma-water explosive interaction involved the UK_E carbonate aquifer. Then, during diatreme propagation within the fault zone, repeated explosions occurred toward shallower levels, resulting in continuous recycling (i.e., increasing fragmentation, rounding and thermal whitening) of entrained wall-rock lithics (UK_E and FFS). Eventually, the eruption-feeding shallower explosions also involved near-surface or locally outcropping Lower Cretaceous Group limestones (LK).

Further indications are given by the analysis of textural features of entrained carbonate lithics (Fig. 7). The null (or very low) degree of whiteness defines a “cold cluster”, also characterized by increasing rounding with fining clast size, which is related to syn-eruptive entrainment at near-surface levels (<500 m depth), without significant thermal magma-clast interaction. On the other hand, the “hot cluster” is defined by peculiar trends of increasing whitening parallel to progressive attrition and/or fragmentation (i.e., decreasing clast size) and/or

rounding, for specific eruptive centers. As a whole, it is apparent that carbonate lithics with different size, roundness and thermal effect features coexist in the eruptive products of individual centers, thus indicating a range of contact times with the magma heat source, as well as multiple lithic entrainment depths (as also testified by the occurrence of near-surface accessory tuffs). Repeated, discrete phreatomagmatic fragmentation events might have occurred at progressively shallower levels during magma ascent (Valentine et al., 2015), from deep-seated PUO limestones (late Aptian-early Cenomanian) upward (Fig. 3, 8). Even lithics with the same composition (e.g., the UK_L Albian-Cenomanian limestones at Fosso di Monteacuto) may show different paths, i.e.: i) increasing rounding (from very angular to rounded) with decreasing size ("cold cluster" Fig. 7), possibly due to syn-eruptive, near-surface fragmentation and transport; ii) incipient to moderate thermal effect with decreasing size and increasing rounding, possibly indicating progressive recycling during clast path to surface; iii) strong thermal effect with reduced grain size and scarce rounding, possibly related to multiple phreatomagmatic fragmentation events from deep-seated to near-surface magma-water interaction levels.

Carbonate clasts were thus entrained and/or recycled through multiple, progressively shallower, discrete fragmentation events during the dyke path to surface, resulting in step-wise fining, rounding and whitening (Fig. 10). Eventually, they were erupted by the most efficient explosions at optimal scaled depth (i.e., physical depth scaled against explosion energy; Graettinger et al., 2014; usually shallower than 200–250 m) that vent to the surface. Hence, in light of recent views on maar-diatreme evolution (White & Ross, 2011; Valentine & White, 2012; Valentine et al., 2015), the appearance of deepest-seated lithics (i.e., Lower Cretaceous Group in the VVF case) at surface is essentially related to multiple fragmentation and mixing processes during the lifetime of a diatreme.

The occurrence of cored lapilli indicates the presence of finely brecciated wall rock domains, pervasively intruded by mafic magmas (or rock fragments entrained along dike/conduit walls). By analogy with the Colli Albani examples (Sottili et al., 2009, 2010), the dominant type of enclosed lithic clast varies from one to another eruptive center. Irregular scoria shells including multiple lithic fragments (e.g. Patrica), possibly originated as magma raised into the root zone of a maar-diatreme and intruded wall rock debris (Lorenz et al., 2002). On the other hand, rounded cored scoria clasts originated when single wall rock fragments were entrained by a low-viscosity magma and erupted with an adhering quenched rim of melt (Rosseel et al., 2006), indicating that the melt was well above the glass transition temperature, a significant temperature difference existed between melt and lithic core at the initial contact, and the time span between lithic entrainment and eruption was shorter than that required for re-melting the quenched rim. Following Sottili et al. (2009, 2010), the observed direct linear correlations between the thickness of the enclosing shell vs. the radius of the lithic core supports inferences on the modes and timing of lithic entrainment, along with constraints to the syn-eruptive thermal state of wall-rocks. Besides a wide scatter due to specific trends for different lithic cores (i.e., carbonate, lava and xenocrysts), overall data from carbonate cores (Fig. 7) indicate relatively low entrainment temperatures (mostly <50°C; similar to the Prata Porci monogenetic maar; Sottili et al., 2009, 2010). This estimate is consistent with an episodic intrusion of a mafic magma dyke in a shallow environment, i.e. ca. 0.5-2 km depth, in agreement with our tectono-stratigraphic reconstructions and the 25°/km present-day geothermal gradient below VR (Boni et al., 1980).

Our findings bear implications on volcanic hazard assessment in the densely populated areas of VR and adjoining Pontina Plain and Middle Latin Valley (~ 0.4 million people over 500 km^2). Due to enduring quiescence since at least 230 ka, the VVF has been so far disregarded for

volcanic risk evaluation. However, a number of volcanic regions worldwide (that also include hydromagmatic centers) recall that phreatomagmatic eruptions, isolated in space and time, may occur after very long quiescence periods (even in the order of 10^5 yrs; e.g., Tchamabé et al., 2016). For instance, at the Quaternary Mt. Vulture volcano, located at the eastern thrust front of the southern Apennine chain, eruptive activity resumed after ca. 300 kyrs of quiescence, originating the Monticchio maars (Principe, 2006).

Even more so, hydrothermally and seismically active areas surrounding VR (e.g., Boni et al., 1980; Duchi et al., 1991; Bono, 1995; INGV seismic catalogue at http://iside.rm.ingv.it/) may potentially host in the future sites of phreatic or even phreatomagmatic events that might likely occur at the intersection of major high-angle normal faults and the ENE volcano-tectonic trend, even in areas where no evidence of previous volcanic activity is known (such as the Pontina Plain along the westward continuation of the ENE volcanic trend).

6. Concluding remarks

New data shed light on the structure of the northern Volsci Range (VR) fold-and-thrust belt and nearby Middle Latin Valley graben, and its relationships with the Volsci Volcanic Field (VVF). Within the network of VVF eruptive centers, we recognized a first-order structural pattern at a regional scale, defined by two clusters of magmatic and phreatomagmatic centers: a NNE-trending cluster, which we consider as the surface expression of deep-seated, high-angle, Mesozoic rift faults (i.e., Ancona-Anzio and Ortona-Roccamonfina lines) of the upper plate, and a ENE-trending one, associated with a lateral slab-tear due to the differential retreat of the subducting Adriatic slab. The latter primarily controlled the fast ascent of small-volume, nearly

primary, magma batches from the mantle source (sort of "bullet eruptions"), as typical of "tectonically controlled volcanic fields" (Valentine and Perry, 2007). On these grounds, the lineaments hosting enduring VVF eruptive activity and, in particular, the ENE-trending one, extending across the whole volcanic field, may be interpreted as the re-activation of a subsidiary crustal structure of the major 41st and 42nd parallel discontinuities,

The superposition of second-order orogenic structures (mainly thrusts and normal faults) controlled the local 3-D distribution pattern and activity styles of volcanic centers and, in particular, the multiple depth levels of magma-water explosive interaction within a stratified carbonate aquifer, consistent with textural indications from entrained lithics and cored scoria lapilli. Specifically, the variable degrees of rounding, whitening and comminution of carbonate lithics define different degrees of magma-wall rock thermal interaction, phreatomagmatic fragmentation, and clast recycling at deep (-800 to -2300 m below the present day surface) and near-surface (<500 m depth) levels along the magma ascent path. Finally, a third-order of structures provides neo-tectonic evidence of active faulting even long after VVF eruptive activity.

Our study sets the groundwork for ongoing volcanological, petrological and geochronological studies, aiming at defining in detail the VVF eruptive history and related magma sources. Moreover, our findings bear implications on volcanic hazard assessment in the densely populated (> 0.4 million people) areas of VR and adjoining Pontina Plain and Middle Latin Valley.

Declaration of interests
The authors declare that they have no known competing financial interests or personal relationships that could have appeared to influence the work reported in this paper.

Acknowledgments, Samples, and Data

This work is dedicated to the memory of Professor Carlo Boni, who planted the seed of our curiosity in the study of the Volsci Range, teaching us care for details and control over the big picture. We acknowledge the very helpful suggestions by Karoly Németh and an anonymous reviewer. We are grateful to Laurent Jolivet, Esmeralda Caus, Mariano Parente, Giuseppe Vico, Michele Di Filippo, Alexandra Kushnir, and Angelo Giuliani for their support. Funding by Progetti di Ateneo 2016 (C. Doglioni) and 2017 and 2019 (C. Doglioni and E. Carminati) and by the Spanish Ministry of 'Economía y Competitividad' (project CGL2012-33160) is acknowledged.

References

Accordi, B., Segre, A.O., Cocozza, T., Angelucci, A., Sirna, G., & Farinacci, A. (1966). Sheet 159 Frosinone of the Geological Map of Italy at l:100'000. (2nd edition). Servizio Geologico d' Italia, Roma.

Acocella, V., Faccenna, C., Funiciello, R. (1996). Elementi strutturali della media Valle Latina. Bollettino della Società Geologica Italiana, 1996, vol. 115(3), 501–518.

Acocella, V., & Funiciello, R. (2006). Transverse systems along the extensional Tyrrhenian margin of central Italy and their influence on volcanism. Tectonics, 25(2).

Alberti, A., Bergomi, C., Catenacci, V., Centamore, E., Cestar, G., Chiocchini, M., Chiocchini, U., Manganelli, V., Molinari-Paganelli, V., Panserl-Crescenzi, C., Salvati, L., & Tilia Zuccari, A. (1975). Note illustrative del Foglio 389 Anagni. Carta Geologica d'Italia 1:50.000. Servizio Geologico d'Italia, Roma.

Andrews, R. G., White, J. D., Dürig, T., & Zimanowski, B. (2014). Discrete blasts in granular material yield two-stage process of cavitation and granular fountaining. Geophysical Research Letters, 41(2), 422-428.

Angelucci, A., Devoto, G., & Farinacci, A. (1963). Le" argille caotiche" di Colle Cavallaro a est di Castro dei Volsci (Frosinone). Geologica Romana, 2, 305-329.

Angelucci, A. (1966a). Tectonic marks on pebbles of Middle Latina Valley. Geologica Romana 5, 313–322.

Angelucci, A. (1966b). La serie miocenica della Media Valle Latina. Geologica Romana 5, 425–452.

Angelucci, A., Brotzu, P., Civitelli, G., Morbidelli, L., & Traversa, G. (1974). Il vulcanismo pleistocenico della media Valle Latina (Lazio). Caratteristiche petrografiche e geologiche dei principali affioramenti lavici. Geologica Romana 13, 83–123.

Beaudoin, A., Augier, R., Jolivet, L., Jourdon, A., Raimbourg, H., Scaillet, S., & Cardello, G. L. (2017). Deformation behavior of continental crust during subduction and exhumation: Strain distribution over the Tenda massif (Alpine Corsica, France). Tectonophysics, 705, 12-32.

Bernoulli, D. (2001). Mesozoic–Tertiary carbonate platforms, slopes and basins of the external Apennines and Sicily. In: Vai, G.B., Martini, P. (Eds.), Anatomy of an Orogen: The Apennines and Adjacent Mediterranean Basins. Kluwer Academic Publishers, Dordrecht, 307–325.

Blaikie, T. N., van Otterloo, J., Ailleres, L., Betts, P. G., & Cas, R. A. F. (2015). The erupted volumes of tephra from maar volcanoes and estimates of their VEI magnitude: examples from the late Cenozoic Newer Volcanics Province, south-eastern Australia. Journal of Volcanology and Geothermal Research, 301, 81-89.

Boari, E., & Conticelli, S. (2007). Mineralogy and petrology of associated Mg-rich ultrapotassic, shoshonitic, and calc-alkaline rocks: the Middle Latin Valley monogenetic volcanos, Roman Magmatic Province, Southern Italy. The Canadian Mineralogist, 45(6), 1443-1469.

Boari, E., Tommasini, S., Laurenzi M.A., & Conticelli S. (2009). Transition from Ultrapotassic Kamafugitic to Sub-alkaline Magmas: Sr, Nd, and Pb Isotope, Trace Element and 40Ar-39Ar Age Data from the Middle Latin Valley Volcanic Field, Roman Magmatic Province, Central Italy. Journal of Petrology 7, 1327–1357.

Boni, C., Bono, P., Calderoni, G., Lombardi, & S., Turi, B. (1980). Indagine idrogeologica e geochimica sui rapporti tra ciclo carsico e circuito idrotermale nella Pianura Pontina. Geologia Applicata e Idrogeologia 15, 204–247.

Bono, P. (1995). The sinkhole of Doganella (Pontina Plain, Central Italy). Environmental Geology, 26(1), 48–52.

Butler, R. W., Tavarnelli, E., & Grasso, M. (2006). Structural inheritance in mountain belts: an Alpine–Apennine perspective. Journal of Structural Geology, 28(11), 1893-1908.

Capelli, G., Mastrorillo, L., Mazza, R., Petitta, M., Baldoni, T., Banzato, F., & Teoli, P. (2012). Carta Idrogeologica del Territorio della Regione Lazio, scala 1: 100.000 (4 fogli). Regione Lazio, SELCA Firenze.

Cardello, G.L., & Doglioni, C. (2015). From Mesozoic rifting to Apennine orogeny: The Gran Sasso range (Italy). Gondwana Research 27, 1307–1334.

Carminati, E., & Doglioni, C. (2012). Alps vs. Apennines: the paradigm of a tectonically asymmetric Earth. Earth-Science Reviews, 112(1-2), 67-96.

Carminati, E., Fabbi, S., & Santantonio, M. (2014). Slab bending, syn-subduction normal faulting, and out-of-sequence thrusting in the Central Apennines. Tectonics, 33(4), 530-551.

Castellarin, A., Colacicchi, R., Praturlon, A. and Cantelli, C. (1982). The Jurassic-Lower Pliocene history of the Ancona-Anzio line (central Italy). Memorie della Società Geologica Italiana, 24, 325-336.

Centamore, E., Fumanti, F., & Nisio, S. (2002). The central-northern Apennines geological evolution from Triassic to Neogene time. Bollettino Società Geologica Italiana, Vol. Spec., 1, 181-197.

Centamore, E., Di Manna, P., & Rossi, D. (2007). Kinematic evolution of the Volsci Range: a new overview. Italian Journal of Geosciences 126, 159–172.

Centamore, E., Dramis, F., Di Manna, P., Fumanti, F., Milli S., Rossi, D., Palombo, M.R., Palladino, D.M., Trigila, R., Zanon, V., Chiocchini, M., Didaskalou, P., Potetti, M., & Nisio, S. (2010). Note illustrative del Foglio 402 Ceccano. Carta Geologica d'Italia 1:50.000. Servizio Geologico d'Italia, Roma.

Chiocchini, M., & Mancinelli, A. (1977). Microbiostratigrafia del Mesozoico in facies di piattaforma carbontica dei Monti Aurunci (Lazio Meridionale). Studi Geologici Camerti 3, 109–152.

Chiocchini, M., Chiocchini, R.A., Didaskalou, P., & Potetti, M. (2008). Ricerche micropaleontologiche e biostratigrafiche sul Mesozoico della piattaforma carbonatica laziale-abruzzese (Italia centrale). Memorie Descrittive Carta Geologica d'Italia 84, 5–170.

Cipollari, P., & Cosentino, D. (1995). Miocene unconformities in the central Apennines: geodynamic significance and sedimentary basin evolution. Tectonophysics 252, 375–389.

Civitelli, G., Funiciello, R., & Lombardi, S. (1970). Alcune considerazioni sulla genesi della «Pietra Paesina». Geologica Romana, 9, 195-204.

Consorti, L., Frijia, G., & Caus, E. (2017). Rotaloidean foraminifera from the Upper Cretaceous carbonates of Central and Southern Italy and their chronostratigraphic age. Cretaceous Re-search 70, 226-243.

Cosentino, D., Cipollari, P., Di Donato, V., & Sgrosso, I. (2002). The Volsci Range in the kinematic evolution of the northen and southern Apennine orogenetic system. Italian Journal of Geosciences, Volume speciale 1, 209–218.

Danese, E., & Mattei, M. (2010). The sedimetary substrate of the Colli Albani volcano. In: Funiciello, R. and Giordano, G. (Eds). The Colli Albani volcano. Geological Society, London, Special Publication of IAVCEI 3, 107–139.

De Benedetti, A. A., Caprilli, E., Rossetti, F., & Giordano, G. (2010). Metamorphic, metasomatic and intrusive xenoliths of the Colli Albani volcano and their significance for the reconstruction of the volcano plumbing system. The Colli Albani volcano. Geological Society of London, Special Publication IAVCEI, 3, 153–176.

De Ritis, R., Pepe, F., Orecchio, B., Casalbore, D., Bosman, A., Chiappini, M., Chiocci, F., Corradino, M., Nicolich, R., Martorelli, E., Monaco, C., Presti, D., & Totaro, C. (2019). Magmatism along lateral slab-edges: insights from the Diamante-Enotrio-Ovidio Volcanic-Intrusive Complex (Southern Tyrrhenian Sea). Tectonics, 38.

Doglioni, C. (1991). A proposal for the kinematic modelling of W-dipping subductions-possible applications to the Tyrrhenian-Apennines system. Terra Nova, 3(4), 423-434.

Doglioni, C., Innocenti, F., & Mariotti, G. (2001). Why Mt Etna?. Terra Nova, 13(1), 25-31.

D'Orazio, M., Innocenti, F., Tonarini, S., & Doglioni, C. (2007). Carbonatites in a subduction system: the Pleistocene alvikites from Mt. Vulture (southern Italy). Lithos, 98(1-4), 313-334.

Duchi, V., Paolieri, M., & Pizzetti, A. (1991). Geochemical study on natural gas and water discharges in the Southern Latium (Italy): circulation, evolution of fluids and geothermal potential in the region. J. Volcanol. Geotherm. Res. 47, 221–235.

Ernst, G., Sparks, R. S. J., Carey, S., and Bursik, M. (1996). Sedimentation from turbulent jets and plumes, J. Geophys. Res., 101, 5575-5589.

Fabbi, S., & Smeraglia, L. (2019). Pop-up structure in massive carbonate-hosted fold-and-thrust belt: Insight from field mapping and 2D kinematic model in the central Apennines. Journal of Structural Geology.

Freda, C., Gaeta, M., Palladino, D. M., & Trigila, R. (1997). The Villa Senni Eruption (Alban Hills, central Italy): the role of H2O and CO2 on the magma chamber evolution and on the eruptive scenario. Journal of Volcanology and Geothermal Research, 78(1-2), 103-120.

Freda, C., Gaeta, M., Giaccio, B., Marra, F., Palladino, D. M., Scarlato, P., & Sottili, G. (2011). CO2-driven large mafic explosive eruptions: the Pozzolane Rosse case study from the Colli Albani Volcanic District (Italy). Bulletin of Volcanology, 73(3), 241-256.

Frezzotti, M. L., De Astis, G., Dallai, L., & Ghezzo, C. (2007). Coexisting calc-alkaline and ultrapotassic magmatism at Monti Ernici, Mid Latina Valley (Latium, central Italy). European Journal of Mineralogy, 19(4), 479-497.

Funiciello, R., & Parotto, M. (1978). Il substrato sedimentario nell'area dei Colli Albani: considerazioni geodinamiche e paleogeografiche sul margine tirrenico dell'Appennino centrale. Geologica Romana 17, 233–287.

Gaeta, M., Freda, C., Marra, F., Arienzo, I., Gozzi, F., Jicha, B., & Di Rocco,T. (2016). Paleozoic metasomatism at the origin of Mediterranean ultrapotassic magmas: constraints from time-dependent geochemistry of Colli Albani volcanic products (Central Italy), Lithos, 244, 151-164.

Giordano, G., De Rita, D., Cas, R., & Rodani, S. (2002). Valley pond and ignimbrite veneer deposits in the small-volume phreatomagmatic 'Peperino Albano' basic ignimbrite, Lago Albano maar, Colli Albani volcano, Italy: influence of topography. Journal of Volcanology and Geothermal Research 118, 131–144.

Giordano, G., De Benedetti, A.A., Diana, A., Diano, G., Gaudioso, F., Marasco, F., Miceli, M., Mollo, S., Cas, R.A.F., & Funiciello, R. (2006). The Colli Albani mafic caldera (Roma, Italy): Stratigraphy, structure and petrology. Journal of Volcanology and Geothermal Research 155, 49–80.

Giordano, G., De Benedetti, A. A., Bonamico, A., Ramazzotti, & P., Mattei, M. (2014). Incorporating surface indicators of reservoir permeability into reservoir volume calculations: Application to the Colli Albani caldera and the Central Italy Geothermal Province. Earth-Science Reviews, 128, 75-92.

Graettinger, A. H. (2018). Trends in maar crater size and shape using the global Maar Volcano Location and Shape (MaarVLS) database. Journal of Volcanology and Geothermal Research, 357, 1-13.

Graettinger, A. H., Valentine, G. A., Sonder, I., Ross, P. S., White, J. D., & Taddeucci, J. (2014). Maar-diatreme geometry and deposits: Subsurface blast experiments with variable explosion depth. Geochemistry, Geophysics, Geosystems, 15(3), 740-764.

Gvirtzman, Z., & Nur, A. (1999). The formation of Mount Etna as the consequence of slab rollback. Nature, 401(6755), 782.

Healy, D., Rizzo, R.E., Cornwell, D.G., Farrell, N.J., Watkins, H., Timms, N.G., Gomez-Rivas, E., & Smith, M. (2016). FracPaQ: a MATLAB toolbox for the quantification of fracture patterns. J. Struct. Geol.

Koornneef, J. M., Nikogosian, I., van Bergen, M. J., Vroon, P. Z., & Davies, G. R. (2019). Ancient recycled lower crust in the mantle source of recent Italian magmatism. Nature Communications, 10(1), 1-10.

Le Corvec, N., Spörli, K. B., Rowland, J., & Lindsay, J. (2013). Spatial distribution and alignments of volcanic centers: clues to the formation of monogenetic volcanic fields. Earth-Science Reviews, 124, 96-114.

Lefebvre, N. S., White, J. D. L., & Kjarsgaard, B. A. (2013). Unbedded diatreme deposits reveal maar-diatreme-forming eruptive processes: Standing Rocks West, Hopi Buttes, Navajo Nation, USA. Bulletin of Volcanology, 75(8), 739.

Lorenz, V. (1986). On the growth of maars and diatremes and its relevance to the formation of tuff rings. Bulletin of volcanology, 48(5), 265-274.

Lorenz, V. (1987). Phreatomagmatism and its relevance. Chemical Geology, 62(1-2), 149-156.

Lorenz, V. (2003). Maar–diatreme volcanoes, their formation, and their setting in hard-rock or soft-rock environments. Geolines—J Geol Inst AS Czech Republic 15, 72–83.

Lorenz, V., Suhr, P., & Suhr, S. (2017). Phreatomagmatic maar-diatreme volcanoes and their incremental growth: a model. Geological Society, London, Special Publications, 446(1), 29-59.

Marra, F., Freda, C., Scarlato, P., Taddeucci, J., Karner, D. B., Renne, P. R., Gaeta, M., Palladino, D.M., Trigila, R. & Cavarretta, G. (2003). Post-caldera activity in the Alban Hills volcanic district (Italy): 40 Ar/39 Ar geochronology and insights into magma evolution. Bulletin of Volcanology, 65(4), 227-247.

Marra, F., Castellano, C., Cucci, L., Florindo, F., Gaeta, M., Jicha, B.R., Palladino, D.M., Sottili, G., Tertulliani, A., and Tolomei, C. (2020). Monti Sabatini and Colli Albani: the dormant twin volcanoes at the gates of Rome. Sci Rep 10, 8666.

Mazzarini, F., & D'Orazio, M. (2003). Spatial distribution of cones and satellite-detected lineaments in the Pali Aike Volcanic Field (southernmost Patagonia): insights into the tectonic setting of a Neogene rift system. Journal of Volcanology and Geothermal Research, 125(3-4), 291-305.

McClintock, M., & White, J. D. (2006). Large phreatomagmatic vent complex at Coombs Hills, Antarctica: wet, explosive initiation of flood basalt volcanism in the Ferrar-Karoo LIP. Bulletin of Volcanology, 68(3), 215-239.

Milia, A., & Torrente, M. M. (2015). Tectono-stratigraphic signature of a rapid multistage subsiding rift basin in the Tyrrhenian-Apennine hinge zone (Italy): A possible interaction of upper plate with subducting slab. Journal of Geodynamics 86, 42–60.

Molli, G. (2008). Northern Apennine–Corsica orogenic system: an updated overview. Geological Society, London, Special Publications, 298(1), 413-442.

Németh, K., Martin, U., & Harangi, S. (2001). Miocene phreatomagmatic volcanism at Tihany (Pannonian Basin, Hungary). Journal of Volcanology and Geothermal Research, 111(1-4), 111-135.

Németh, K., & Kósik, S. (2020). Review of explosive hydrovolcanism. Geosciences, 10(2), 44.

Novarese, V. (1943). Il Miocene della Valle Latina, Boll. Del Regio Ufficio Geologico d'Italia, col. LXVIII, Roma.

Palladino, D., Gaeta, M., & Marra, F. (2001). A large K-foiditic hydromagmatic eruption from the early activity of the Alban Hills Volcanic District, Italy. Bulletin of Volcanology, 63(5), 345-359.

Palladino, D.M., Valentine, G.A., Sottili, G., & Taddeucci, J. (2015). Maars to calderas: end-members on a spectrum of explosive volcanic depressions. Front. Earth Sci., Perspective, 3-36, 8 pp., doi: 10.3389/feart.2015.00036.

Parotto, M., & Tallini, M. (2013). Geometry and kinematics of the Montelanico-Carpineto Backthrust (Lepini Mts., Latium) in the hangingwall of the early Messinian thrust front of the central Apennines: implications for the Apennine chain building. Italian Journal of Geosciences 132, 274–289.

Pasquarè, G., Serri, G., & Vezzoli, L. (1985). Carta geologica dell'area della MediaValle Latina. Scala 1:50 000. Progetto finalizzato geodinamica. Sottoprogetto: sorveglianza dei vulcani e rischio vulcanico. In: Carte tematiche sul vulcanismo recente. Milan: Istituto di Geologia, University of Milan.

Peccerillo, A. (2005). Plio-quaternary volcanism in Italy (Vol. 365). Springer-Verlag Berlin Heidelberg.

Pizzi, A., & Galadini, F. (2009). Pre-existing cross-structures and active fault segmentation in the northern-central Apennines (Italy). Tectonophysics, 476(1-2), 304-319.

Powers, M.C. (1953). A new roundness scale for sedimentary particles. Journal of sedimentary Petrology 23, 117–119.

Principe, C. (2006). La geologia del monte Vulture. Consiglio Nazionale delle Ricerche, Italy, 218 pp

Re, G., White, J. D., Muirhead, J. D., & Ort, M. H. (2016). Subterranean fragmentation of magma during conduit initiation and evolution in the shallow plumbing system of the small-volume Jagged Rocks volcanoes (Hopi Buttes Volcanic Field, Arizona, USA). Bulletin of Volcanology, 78(8), 55.

Roduit, N. (2008). JMicroVision: Image analysis toolbox for measuring and quantifying components of high-definition images. JMicroVision Version 1.2.7, 2002-2008.

Romano, M., Manni, R., Venditti, E., Nicosia, U., & Cipriani, A. (2019). First occurrence of a Tylosaurinae mosasaur from the Turonian of the Central Apennines, Italy. Cretaceous Research, 96, 196-209.

Rosenbaum, G., & Piana Agostinetti, N. (2015). Crustal and upper mantle responses to lithospheric segmentation in the northern Apennines. Tectonics, 34(4), 648-661.

Rosenbaum, G., Gasparon, M., Lucente, F. P., Peccerillo, A., & Miller, M. S. (2008). Kinematics of slab tear faults during subduction segmentation and implications for Italian magmatism. Tectonics 27, TC2008.

Ross, P. S., & White, J. D. (2006). Debris jets in continental phreatomagmatic volcanoes: a field study of their subterranean deposits in the Coombs Hills vent complex, Antarctica. Journal of Volcanology and Geothermal Research, 149(1-2), 62-84.

Rosseel, J. B., White, J. D. L., & Houghton, B. F. (2006). Complex bombs of phreatomagmatic eruptions: role of agglomeration and welding in vents of the 1886 Rotomahana eruption, Tarawera, New Zealand. Journal of Geophysical Research: Solid Earth, 111(B12).

Ruch, J., Wang, T., Xu, W., Hensch, M., & Jónsson, S. (2016). Oblique rift opening revealed by reoccurring magma injection in central Iceland. Nature communications, 7, 12352.

Sani, F., Del Ventisette, C., Montanari, D., Coli, M., Nafissi, P., & Piazzini, A. (2004). Tectonic evolution of the internal sector of the Central Apennines, Italy. Marine and petroleum geology, 21(10), 1235-1254.

Santantonio, M., & Carminati, E. (2011). Jurassic rifting evolution of the Apennines and Southern Alps (Italy): Parallels and differences. GSA Bulletin, 123(3-4), 468-484.

Scrocca, D., Carminati, E., Doglioni, C., & Marcantoni, D. (2007). Slab retreat and active shortening along the central-northern Apennines. In Thrust belts and foreland basins (pp. 471-487). Springer, Berlin, Heidelberg.

Sheridan, M. F., & Wohletz, K. H. (1983). Hydrovolcanism: basic considerations and review. Journal of Volcanology and Geothermal Research, 17(1-4), 1-29.

Sirna (1963). Aptian charophyta of southern Latium. Geologica Romana 2, 279–290.

Sottili, G., Taddeucci, J., Palladino, D.M., Gaeta, M., Scarlato, P., & Ventura, G. (2009). Sub-surface dynamics and eruptive styles of maars in the Colli Albani Volcanic District, Central Italy. Journal of Volcanology and Geothermal Research 180, 189–202.

Sottili, G., Taddeucci, J., & Palladino, D.M. (2010). Constraints on magma-wall rock thermal interaction during explosive eruptions from textural analysis of cored bombs. J. Volcanol. Geotherm. Res., 192: 27-34.

Sottili, G., Palladino, D.M., Gaeta, M., & Masotta, M. (2012). Origins and energetics of maar volcanoes: examples from the ultrapotassic Sabatini Volcanic District (Roman Province, Central Italy). Bull. Volcanol. 74, 163–186. http://dx.doi.org/10.1007/s00445-011-0506-8.

Sweeney, M. R., & Valentine, G. A. (2015). Transport and mixing dynamics from explosions in debris-filled volcanic conduits: numerical results and implications for maar-diatreme volcanoes. Earth and Planetary Science Letters, 425, 64-76.

Tadini, A., Bonali, F. L., Corazzato, C., Cortés, J. A., Tibaldi, A., & Valentine, G. A. (2014). Spatial distribution and structural analysis of vents in the Lunar Crater Volcanic Field (Nevada, USA). Bulletin of Volcanology, 76(11), 877.

Taddeucci, J., Sottili, G., Palladino, D. M., Ventura, G., & Scarlato, P. (2010). A note on maar eruption energetics: current models and their application. Bulletin of Volcanology, 72(1), 75-83.

Tchamabé, B. C., Kereszturi, G., Németh, K., & Carrasco-Núñez, G. (2016). How Polygenetic are Monogenetic Volcanoes: Case Studies of Some Complex Maar-Diatreme Volcanoes. In Updates in Volcanology - From Volcano Modelling to Volcano Geology. IntechOpen. 355-389.

Trippanera, D., Acocella, V., Ruch, J., & Abebe, B. (2015). Fault and graben growth along active magmatic divergent plate boundaries in Iceland and Ethiopia. Tectonics, 34(11), 2318-2348.

Valentine, G. A., & White, J. D. (2012). Revised conceptual model for maar-diatremes: Subsurface processes, energetics, and eruptive products. Geology, 40(12), 1111-1114.

Valentine, G. A., & Cortés, J. A. (2013). Time and space variations in magmatic and phreatomagmatic eruptive processes at Easy Chair (Lunar Crater Volcanic Field, Nevada, USA). Bulletin of Volcanology, 75(9), 752.

Valentine, G. A., & Perry, F. V. (2007). Tectonically controlled, time-predictable basaltic volcanism from a lithospheric mantle source (central Basin and Range Province, USA). Earth and Planetary Science Letters, 261, 201-216.

Valentine, G. A., Sottili, G., Palladino, D. M., & Taddeucci, J. (2015). Tephra ring interpretation in light of evolving maar–diatreme concepts: Stracciacappa maar (central Italy). Journal of Volcanology and Geothermal Research, 308, 19-29.

Valentine, G. A., Cortés, J. A., Widom, E., Smith, E. I., Rasoazanamparany, C., Johnsen, R., Briner, J. P., Harp, A. G., & Turrin, B. (2017). Lunar crater volcanic field (reveille and pancake ranges, basin and Range Province, Nevada, USA). Geosphere, 13(2), 391-438.

Washington, H.S. (1906). The Roman comagmatic region. Carnegie Institute, Washington 145 p.

White, J. D., & Ross, P. S. (2011). Maar-diatreme volcanoes: a review. Journal of Volcanology and Geothermal Research, 201(1-4),

Wohletz, K., & Heiken, G. (1992). Volcanology and geothermal energy. United States: N. p., 1992. Web.

Figure captions

Figure 1. a) Sketch tectonic map of central Italy, showing the location of the study area in the northern Volsci Range and the volcanic setting of the Roman Province (modified after Bernoulli, 2001); b) lithospheric-scale cross-section beneath central Apennines (modified after Carminati et al., 2014), showing magma injection and eruption associated with the Volsci Volcanic Field (VVF) in the context of W-directed subduction of the Adriatic Plate. Ages in italics show the time window (beginning/end) of accretion into the wedge related to each tectonic unit.

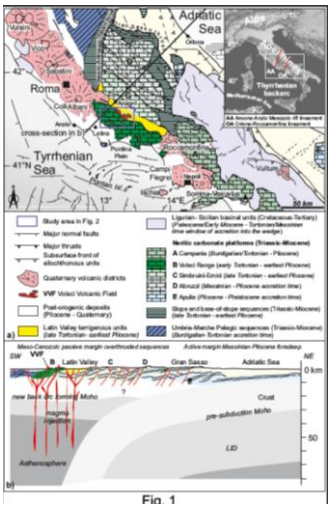

Figure 2. Geological sketch map of the northern Volsci Range and adjoining Middle Latin Valley, including locally sourced VVF eruptive centers. The traces of the seismic line (dotted) of Fig. 8 and geological cross-sections (A-B and C-D) of Fig. 9 are also shown.

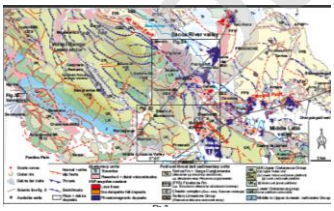

Figure 3. Composite stratigraphic logs of the northern Volsci Range mountain backbone and Middle Latin Valley, correlated to the Geological Map of Italy (Sheet 402-Ceccano; Centamore et al., 2010). On

the right side, the biostratigraphic ranges of the fossil-bearing carbonate lithics collected from the VVF phreatomagmatic deposits (see the Results Section).

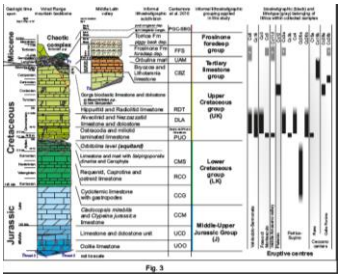

Figure 4. a-b) Panoramic view over the VR mountain backbone along the southern part of the A-B geological cross-section (see Fig. 2 for location); c) the Orbitolina level between the Lower Cretaceous well-bedded limestone (LK) and the upper Albian-Cenomanian limestone (UK), exposed along the southern slope of Semprevisa Mt. (41°34'3.28"N; 13°04'14.12"E); d) karstic cruston lineated by the eastward overthrusting of the Upper Volsci Unit, cross-cut by high angle en-echelon fractures (41°34'47"N; 13°13'59"E); e) panoramic view of NW-striking normal faults dissecting the Volsci Range fold-and-thrust structure; the stereoplot of kinematic indicators and local structural elements is also shown (measured near Supino; 41°36'14"N; 13°10'48"E).

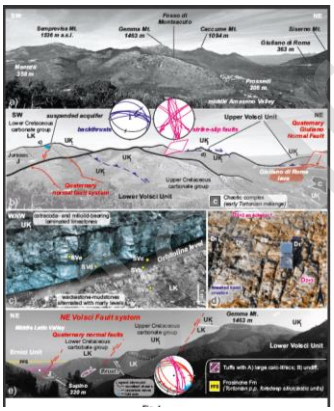

Figure 5. Volcano-tectonic map of VVF, showing the first-order trends, as deduced from clusters of rooted eruptive centers (grey areas), and the second-order trends, defined by eruptive centers associated

with major faults reaching the surface (yellow areas) and with minor fault segments (dashed ellipses). Downright, the rose diagram shows the strike of the two order trends (n= number of measurements).

Figure 6. a) Stereo-plots of volcano-tectonic second-order trends, highlighted by representative structural data on major fault zones (red: faults; orange: fractures crosscutting phreatomagmatic deposits), measured at Valvisciolo (41°34'12.08"N; 12°58'40.98"E and 41°34'46"N; 12°58'28"), Roccagorga (41°31'18"N; 13°8'26"E), Giuliano di Roma (41°32'17"N; 13°16'54"E) and Patrica (41°35'29.69"N; 13°14'31.01"E) localities; rose-diagrams from structural and geomorphic elements (b: all faults from the volcano-tectonic map of Fig. 5; c: related to the third-order trends in the Middle Latin Valley-Ceccano area).

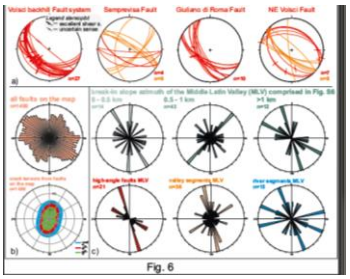

Figure 7. a) Example of *peperino* texture in VVF phreatomagmatic deposits (sample CC31; Patrica center), showing a cored scoria lapilli and carbonate lithics with variable degrees of thermal interaction (from thermally altered edges to zoned contact marble); b) hand draw of image a, outlining the juvenile shells in a cored scoria lapilli; c) example of core and shell from image b after thresholding and binarization; d) shell thickness and core equivalent radius as calculated from the binary image c; e) plots of core radius (a) vs. crown thickness (Δr) for cored-lapilli from selected phreatomagmatic deposits; colored dots represent the entrained carbonate lithics, while gray dots in the background are representative of other core lithologies. Thermal gradients are reported, according to Sottili et al., 2010; image (f) and hand draw (g) of a zoned, rounded carbonate lithic showing evidence of successive breakage and thermal alteration along the new-formed edges; h) textural characterization of carbonate lithics from VVF eruptive centers. The ternary diagram shows lithic clast sizes (measured along the mean axis, representative of phreatomagmatic fragmentation plus attrition during diatreme transport), the

degree of whiteness (representative of thermal interaction), and roundness (representative of attrition due to recycling during diatreme transport). All values are normalized to 100% (see Materials and methods). "Hot" (dotted) and "cold" (gray area) clusters are highlighted (see Section 4.7 for explanation). Key to reading: for instance, a single lithic clast from Fosso di Monteacuto (pointed by black arrow) is characterized by: i) a size that is 74% of the maximum clast size in the sample; ii) a degree of roundness of 1 (according to the scale of Powers, 1953), which is 7% of a clast with the highest rounding value of 6; iii) a whiteness of 19% relative to a pure white clast (value of 100% on a chromatic scale; i.e. maximum thermal effect). In comparison, a clast with similar size in the cold cluster has 0% whiteness (i.e., thermally unaltered).

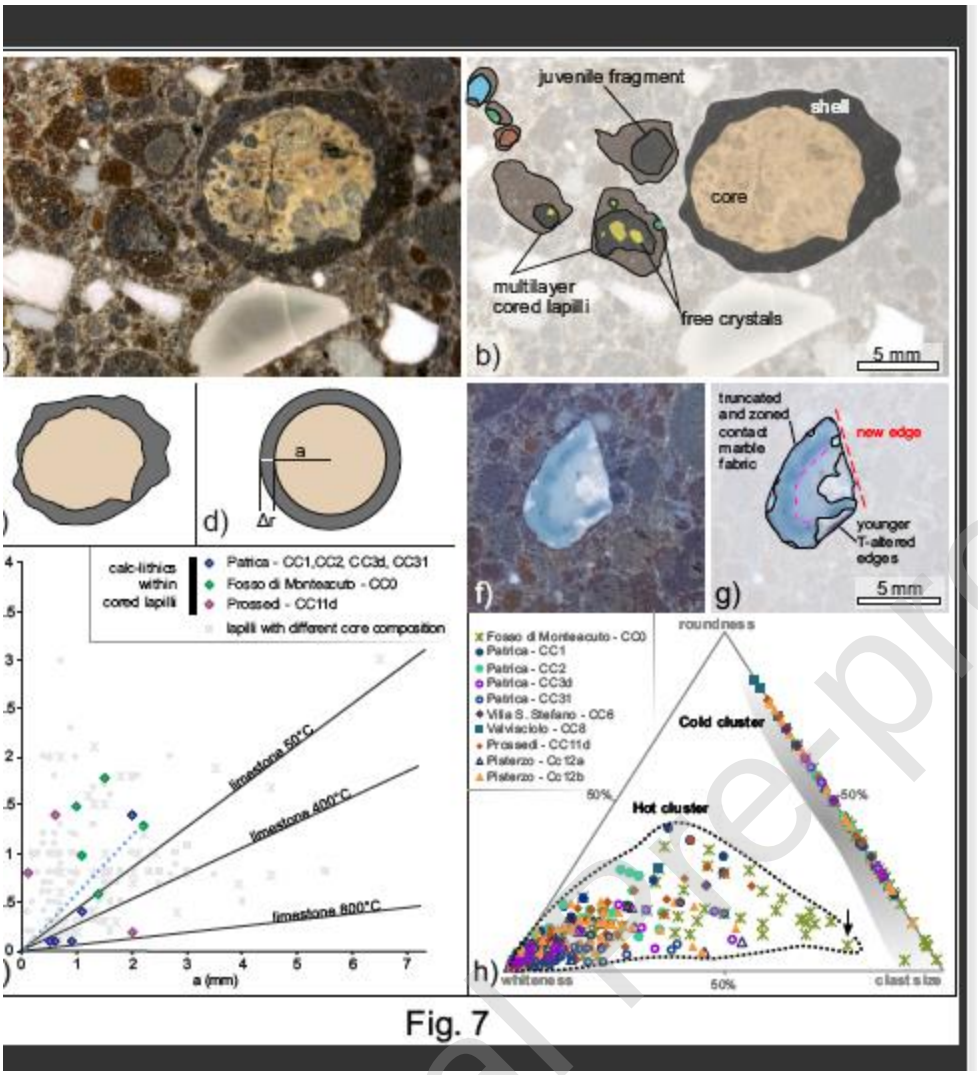

Fig. 7

Figure 8. Two-times travel (TWT) seismic line FR306-80 (right, interpreted), also showing the projection of the Frosinone-001 well (from www.videpi.com) and of the Ripi I well (Novarese, 1943).

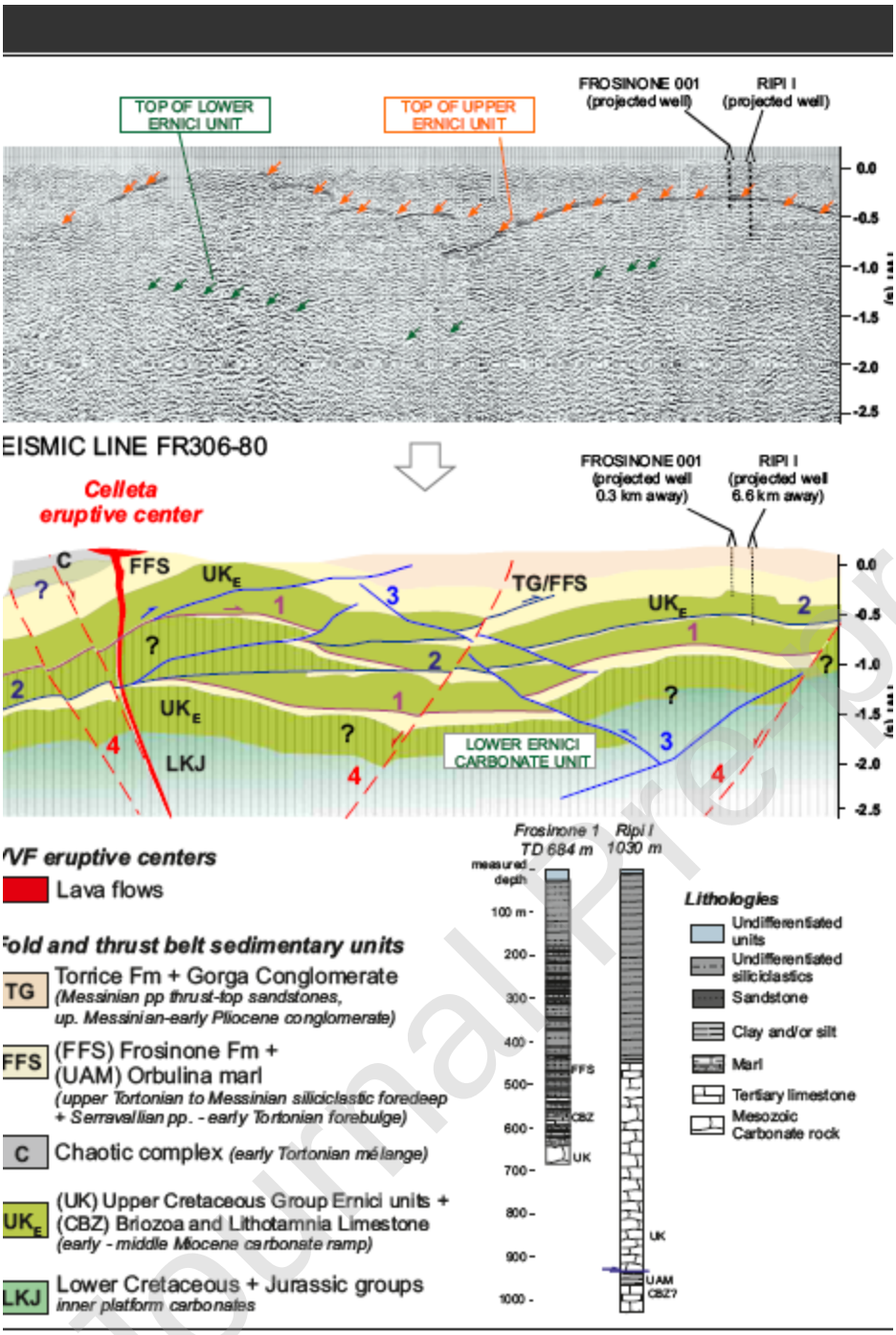

Fig. 8

Figure 9. Geological cross-section AB, showing the fold-and-thrust belt architecture of the VVF substrate between Maenza and Tecchiena. Numbers 1-2-3 refer to the relative time of thrusting from the oldest/highest to the youngest/lowest thrust; number 4 refers to the subsequent normal faulting. The possible sites of magma-water interaction within fault-controlled diatremes are also shown.; Geological

cross-section CD between Prossedi and Pofi. See Fig. 2 for the traces of the seismic line and geological cross-sections.

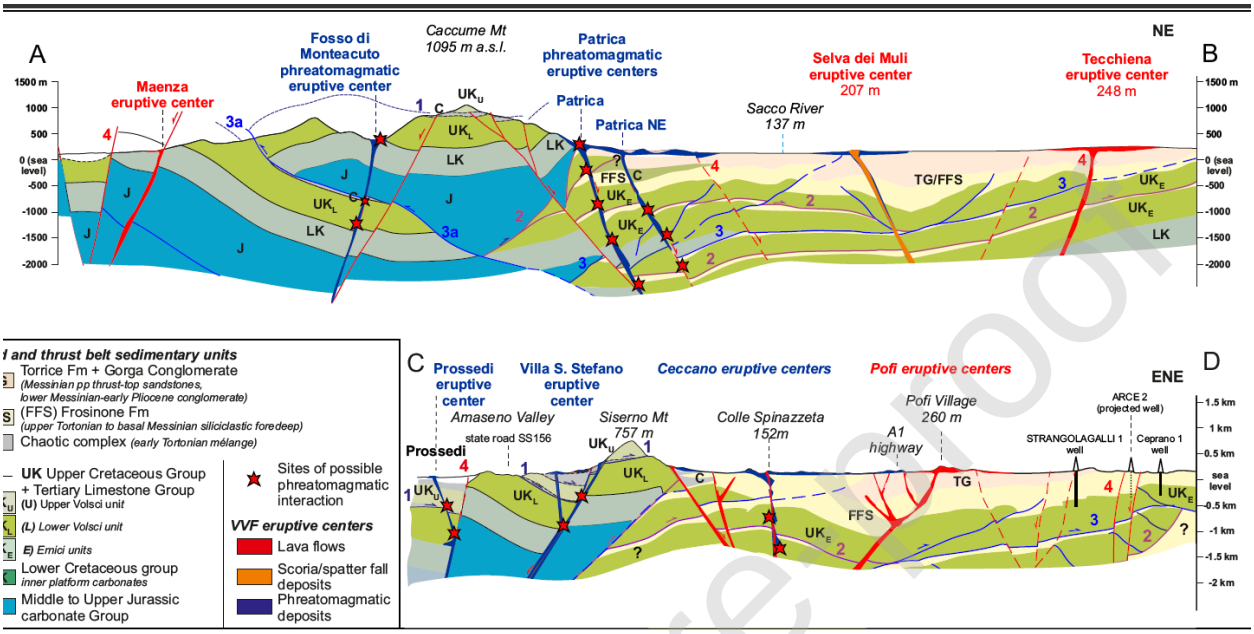

Fig. 9

Figure 10. a) Sketch model for the sub-surface and eruptive processes of the VVF maar-diatremes. Major high angle normal faults (red lines) drove magma injection from the mantle source and controlled the sites of magma-water explosive interaction, eventually acting as paths to surface during phreatomagmatic eruptions. b) Cartoon highlighting the stratigraphic and structural control of carbonate wall rocks over diatreme processes: multiple levels of magma-water interaction resulted in several steps of magma fragmentation and textural evolution (due to thermal interaction and recycling) of entrained carbonate lithics.